

Water-Templated Growth of Interfacial Superglue Polymers for Tunable Thin Films and In Situ Fluid Encapsulation

Venkata S. R. Jampani, Miha Škarabot, Urban Mur, Damien Baigl, Ulrich Jonas, Jan P. F. Lagerwall, Miha Ravnik, and Manos Anyfantakis*

Thin polymer films (TPFs) are indispensable elements in numerous technologies ranging from liquid encapsulation to biotechnology to electronics. However, their production typically relies on wet chemistry involving organic solvents or chemical vapor deposition, necessitating elaborate equipment and often harsh conditions. Here, an eco-friendly, fast, and facile synthesis of water-templated interfacial polymers based on cyanoacrylates (superglues, CAs) that yield thin films with tailored properties is demonstrated. Specifically, by exposing a cationic surfactant-laden water surface to cyanoacrylate vapors, surfactant-modulated anionic polymerization produces a manipulable thin polymer film with a thickness growth rate of 8 nm min^{-1} . Furthermore, the shape and color of the film are precisely controlled by the polymerization kinetics, wetting conditions, and/or exposure to patterned light. Using various interfaces as templates for film growth, including the free surface of drops and soap bubbles, the developed method advantageously enables in situ packaging of chemical and biological cargos in liquid phase as well as the encapsulation of gases within solidified bubbles. Simple, versatile, and biocompatible, this technology constitutes a potent platform for programmable coating and soft/smart encapsulation of fluids.

micrometers. Due to their reduced dimensions, TPFs exhibit unique properties and serve as ideal platforms for exploring fundamental soft matter questions, e.g., the confinement effect on the dynamics of the constituent chains,^[1] or for developing technologies ranging from biological applications^[2] to anticorrosion coatings,^[3] water-repellent fabrics,^[4] and wearable electronics.^[5] This multitude of applications necessitates the development of methods delivering TPFs with well-controlled properties that are simple and cost-effective. Physical methods like spin-^[6] and dip-coating^[7] or layer-by-layer assembly^[8] rely on dissolving a prefabricated polymer, which is then deposited on a substrate. Despite their capability to control film thickness, such methods rely on solvents, often expensive or harmful organic liquids requiring special handling. Chemical vapor deposition methods overcome this limitation by employing in situ

polymerization of reactants through the gas phase directly above the substrate.^[9] Despite the excellent control of film properties, demanding conditions, typically low pressure and high temperature, are required. Besides the specialized equipment needed, this imposes constraints on the utilized materials and the process scaling up. Plasma-enhanced chemical vapor deposition uses

1. Introduction

Thin polymer films (TPFs) are layers of polymer materials with a uniform thickness from a few nanometers to

V. S. R. Jampani, J. P. F. Lagerwall, M. Anyfantakis
Department of Physics and Materials Science
University of Luxembourg
Luxembourg L-1511, Luxembourg
E-mail: anyfas.com@gmail.com

V. S. R. Jampani, M. Škarabot
Condensed Matter Physics Department
Jožef Stefan Institute
Ljubljana 1000, Slovenia

U. Mur, M. Ravnik
Faculty of Mathematics and Physics
University of Ljubljana
Ljubljana 1000, Slovenia

D. Baigl
PASTEUR
Department of Chemistry
École Normale Supérieure
PSL University
Sorbonne Université
CNRS
Paris 75005, France

U. Jonas
Department of Chemistry and Biology
University of Siegen
D-57076 Siegen, Germany

 The ORCID identification number(s) for the author(s) of this article can be found under <https://doi.org/10.1002/adma.202408243>

© 2024 The Author(s). Advanced Materials published by Wiley-VCH GmbH. This is an open access article under the terms of the [Creative Commons Attribution-NonCommercial](#) License, which permits use, distribution and reproduction in any medium, provided the original work is properly cited and is not used for commercial purposes.

DOI: 10.1002/adma.202408243

reactive plasma species to activate monomers at lower temperatures, enabling TPF synthesis even at atmospheric pressure,^[10] as shown by polymerizing monomers inside sessile droplets on a substrate.^[11] Despite the great potential of plasma deposition methods, the strong dependence of film quality on operating parameters and the need for noble gases limit their widespread use.

We envisaged that using CAs, readily available monomers that rapidly polymerize under environmental conditions, would be a practical strategy for preparing TPFs. CAs and their polymers (PCAs) are commercially important due to their suitability for plentiful applications.^[12] Methyl and ethyl cyanoacrylate (ECA) are industrially valuable because they are the basis of instant adhesives. Larger CAs like butyl and octyl CA are used to close wounds,^[13] partly due to their bacteriostatic properties.^[14] CAs are also used in multiple fields, from fingerprint visualization in forensics^[15] to multifunctional coatings.^[16] The extended utility of CAs stems from their high reactivity. Weak nucleophiles like OH⁻ from the self-dissociation of water molecules (e.g., moisture on a surface) initiate a rapid anionic polymerization, producing large macromolecules almost instantaneously.^[17] The reactivity of CAs, however, makes their use for preparing nanomaterials with controlled morphology challenging.^[18] Overcoming this limitation would allow for further CA exploitation for demanding applications beyond those already shown, e.g., fabricating superhydrophobic surfaces,^[19] recyclable plastics,^[20] and gel polymer electrolytes for flexible lithium batteries.^[21] Besides, PCAs are also biocompatible^[18,22] and biodegradable,^[14,23] which renders them excellent candidates for drug delivery, either as nanospheres^[24] or nanocapsules.^[25] Despite the widespread use of PCA in biomaterial applications^[26] and the vast relevant research,^[27] fundamental chemistry aspects are still being explored.^[28] Hence, if one wishes to unleash the potential of CAs for making precisely engineered materials suitable for emergent applications like liquid encapsulation^[29,30] and flexible electronic paper in color,^[31] new synthesis methods that are well-controlled, versatile, and cost-effective are desired.

To address these challenges, we introduce a concept called WRAPPINGS (Water-based, Room temperature, Atmospheric Pressure Polymerization of INstant Glues controlled by Surfactants). It comprises a minimal system and an eco-friendly method to produce thin PCA films in a straightforward yet highly modular fashion. WRAPPINGS involves the exposure of a cationic surfactant-enriched air–water interface to CA vapor, which initiates anionic polymerization with chain growth confined to the interface and controlled by the surfactants. The resulting TPF has uniform thickness with less than 2% variation over 1 cm² area, which can be accurately tuned by adjusting the reaction time, thanks to a thickness growth rate of ≈ 8 nm min⁻¹. We showcase the potential of this new technology for making and using TPFs on demand with three paradigms. First, by patterning the fluid interface shape and modulating the film thickness, we produce planar films of arbitrary size, shape, and tunable interference color. Second, by combining the polymerization scheme with aqueous templates of different forms, we demonstrate the in situ packaging and manipulation of chemical cargos that is equally applicable to biological ones. Finally, we encapsulate and handle inert and reactive gases in situ by templating the polymerization with soap bubbles.

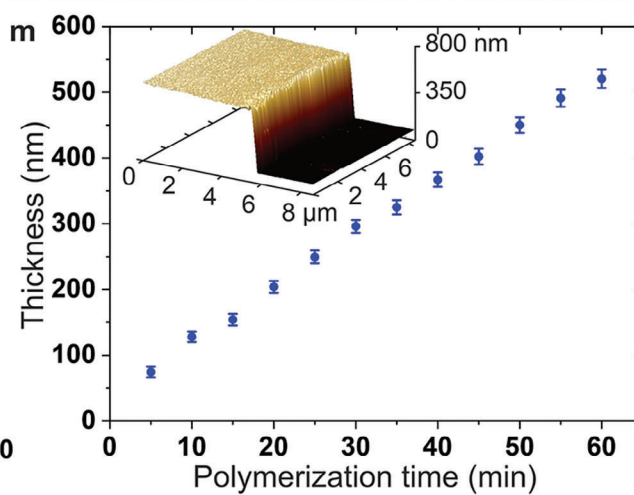
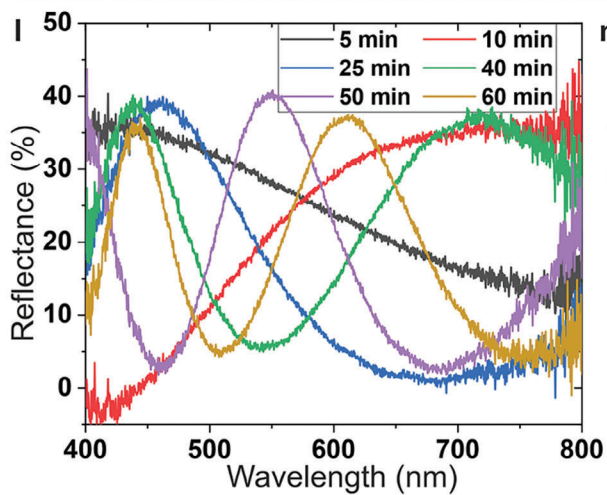
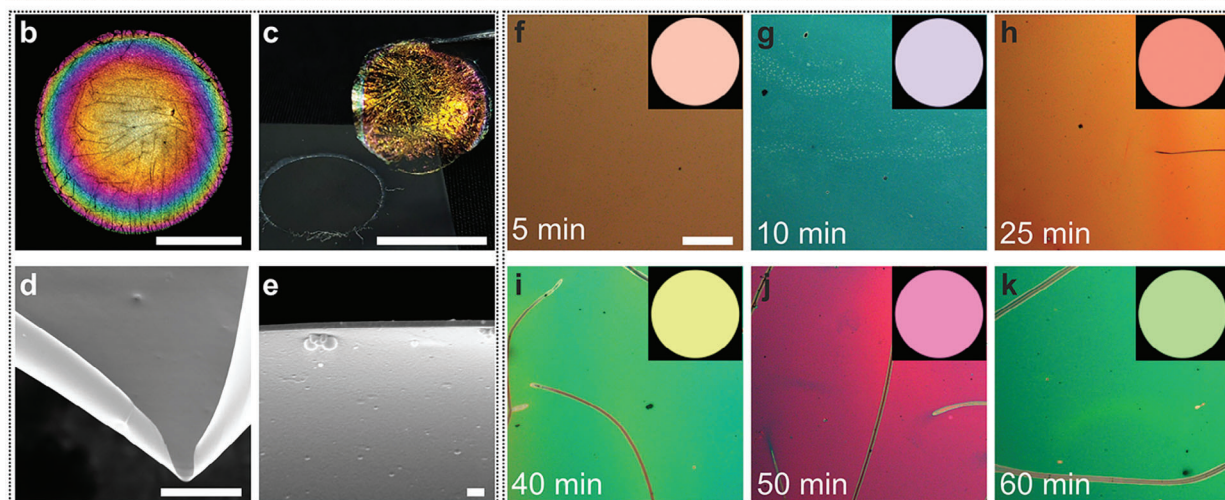
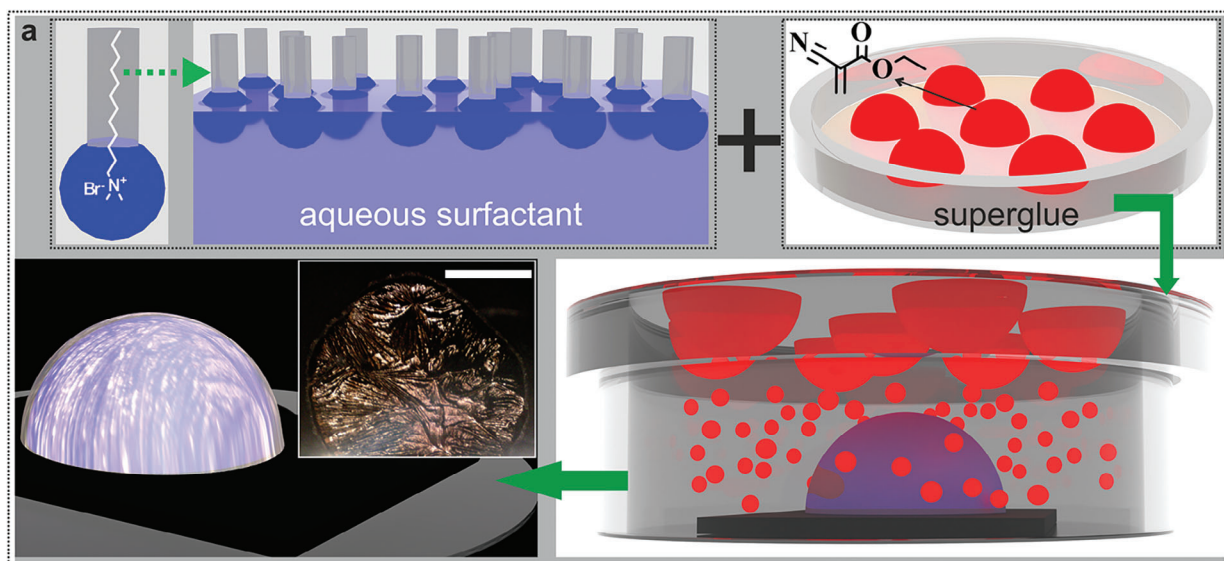
2. Results and Discussion

2.1. PCA Film Formation at a Surfactant-Laden Aqueous Interface Using WRAPPINGS

Figure 1 illustrates the WRAPPINGS concept for making thin PCA films using aqueous cationic surfactant (dodecyltrimethylammonium bromide, DTAB; critical micelle concentration CMC = 13.4 mM^[32]) solutions exposed to CA vapors coming from the air phase. We dispense a DTAB solution drop onto a substrate located in a Petri dish. Once a lid carrying ECA drops is placed on the dish, polymerization begins ($t_{\text{pol}} = 0$, **Figure 1a**). The volatile monomer^[27] quickly evaporates and creates an ECA-rich atmosphere. When ECA molecules reach the fluid interface, water molecules initiate anionic polymerization. The hydroxide anion from self-dissociation of water attacks the β carbon of the double bond, yielding a carbanion, which grows further by subsequent monomer addition.^[33] The rapid polymerization rate is due to the strong electron-withdrawing ester and cyano groups in the α -carbon, which stabilize the carbanion.^[34] **Movie S1** (Supporting Information) shows a highly reflective film appearing first at the center of the drop surface before propagating outward to cover the entire surface. The film color, uniform across its whole surface due to the presence of surfactants (discussed later), is initially silver and progressively changes with t_{pol} , becoming gold at $t_{\text{pol}} = 12$ min (**Figure 1a**, inset), purple, green, and then again purple. A greenish film is observed when the monomer supply is stopped by removing the lid at $t_{\text{pol}} = 30$ min. By removing the solution under the film (**Movie S2**, Supporting Information), we obtain a dry, vividly green poly (ethyl cyanoacrylate) (PECA) film (**SI Appendix**, **Figure S1**, Supporting Information). The film displays varying colors with changing viewing angle. Commercial superglue was used in this experiment, but similar results were obtained with pure ECA (**SI Appendix**, **Figure S2**, Supporting Information).

The versatility of WRAPPINGS is evident in its compatibility with other cyanoacrylates like butyl (BCA) and isopropyl cyanoacrylate (**Figure 1b**, **SI Appendix**, **Figure S3**, Supporting Information). Interestingly, PCA films can be made self-standing by detaching them from the substrate (**Figure 1c**, **Movie S3**, Supporting Information), which facilitates the investigation of their microscopic morphology. Scanning electron microscopy (SEM) images of PECA (**Figure 1d**, **SI Appendix**, **Figure S4**, Supporting Information) and PBCA films (**Figure 1e**, **SI Appendix**, **Figure S5**, Supporting Information) reveal a smooth topography. The softer PBCA film (the bulk PBCA has glass transition temperature $T_{\text{g,PBCA}} = 113$ °C^[12]) exhibits more folding than the more rigid PECA film (bulk PECA, $T_{\text{g,PECA}} = 132$ °C^[12]). This permits the observation of its cross-section, revealing a uniform film thickness ($d_{\text{f}} \approx 308 \pm 19$ nm) along the portion (≈ 70 μm wide) imaged (**SI Appendix**, **Figure S5**, Supporting Information). We confirm the difference in the mechanical properties of TPFs made from these polymers with atomic force microscopy (AFM) measurements of the Young's modulus E , which yielded average values of $E_{\text{PECA}} = 1.6 \pm 0.5$ GPa and $E_{\text{PBCA}} = 0.5 \pm 0.2$ GPa, respectively, for PECA and PBCA films (**Figure S6**, Supporting Information).

To elucidate the influence of reaction time on their properties, we grow a series of PECA films on DTAB solutions by keeping C_{s} fixed and varying t_{pol} (**SI Appendix**, **Figure S7**,



Supporting Information) that are then transferred onto Si wafers (Movie S4, Supporting Information). Reflection microscopy shows that films grown for $t_{\text{pol}} \leq 30$ min become almost wrinkle-free during the transfer process (SI Appendix, Figure S8, Supporting Information), unlike those produced for longer t_{pol} that maintain many wrinkles (SI Appendix, Figure S9, Supporting Information). The wrinkle density increases with t_{pol} , consistent with the observed Young's modulus increase with t_{pol} .^[35] The film color is homogeneous over macroscopic ($\approx \text{cm}^2$) areas and changes with t_{pol} (Figure 1f–k). Microspectroscopy reveals that the color results from broad reflection peaks (Figure 1l, SI Appendix, Figure S10, Supporting Information). We measured the thickness of the films by imaging the edge of the film with AFM (Figure 1m inset, SI Appendix, and Figure S11, Supporting Information). A linear d_f increase with t_{pol} , with a growth rate of $\approx 8 \text{ nm min}^{-1}$, is observed. These findings show that longer t_{pol} results in thicker films, leading to variation in color and an increase in film elasticity. The surface roughness of films grown for different t_{pol} remains unchanged ($R_q \approx 4 \text{ nm}$, SI Appendix, Figure S12, Supporting Information), which agrees with the smooth surface observed with SEM. For these experiments, WRAPPINGS can achieve a d_f range spanning a decade (from $\approx 75 \text{ nm}$ to $\approx 520 \text{ nm}$). The shape of the reflection spectra combined with d_f values on the order of visible light wavelengths suggests that the color-producing mechanism is thin-film interference. To verify this, we calculate the reflectance using the thin-film interference model for plane waves (SI Appendix, Figures S13–S16, Supporting Information). Colors obtained by transforming the calculated spectra into RGB images using the same color transfer functions as in the camera closely match with the experimental micrographs (Figure 1f–k).

2.2. Fundamental Mechanism behind WRAPPINGS

To gain insight into WRAPPINGS, we performed a series of control experiments. First, we replaced DTAB with the cationic surfactant hexadecyltrimethylammonium bromide (CTAB, CMC = 0.92 mM;^[32] SI Appendix, Figure S17a, Supporting Information). Both surfactants produce mechanically robust and colored films, underlining the importance of the amphiphilic nature of the surfactant for the film formation process. In particular, the positively charged head group of the surfactant, located at the air–water interface, creates a 2D template for the growth of the polymer chains. This allows efficient access to the supply of monomers from the gas phase, which directly reach the anionic active sites of the growing chains at the polymer–

water interface (SI Appendix, Figure S18, Supporting Information), electrostatically attracted to the cationic head groups. Second, we challenged the need for cationic surfactants by growing PECA films on bare, ultrapure water. The result is significantly different, as the films are broken, transparent, colorless, and cannot be kept self-standing (SI Appendix, Figure S19, Supporting Information). The film fragility is due to the lower film thickness d_f ($\approx 40 \text{ nm}$ for $t_{\text{pol}} = 20 \text{ min}$), suggesting a comparatively slow TPF growth on pure water (SI Appendix, Supporting Information). This indicates that the dissociation equilibrium between the positive surfactant head group and the active anionic ECA chain end supports larger ion separation and, consequently, faster polymerization rates. In the absence of cationic surfactants, the dissociation equilibrium involves protons more tightly associated with the active sites, thus reducing the polymerization rate. Third, using NaBr solutions as subphase yields colorless, fragile films similar to those grown on pure water (SI Appendix, Figure S17b, Supporting Information). These results rule out a strong influence of well-solvated Br^- anions (also present in the surfactant counterions) on the TPF growth rate. As a fourth control experiment, we investigate the role of electrostatic charge using the anionic surfactant sodium dodecyl sulfate (SDS) in the subphase. This yields colorless TPFs (SI Appendix, Figure S20, Supporting Information), contrary to the color observed with cationic surfactants. These experiments are summarized in SI Appendix, Table S1 (Supporting Information), supporting our hypothesis that interfacial cations are instrumental to the rapid yet controlled PCA film growth. The quaternary ammonium head group of DTAB is bulky, resulting in a weaker association with the active PECA chain end. Additionally, water, a highly polar solvent, promotes ion dissociation. To further scrutinize this hypothesis, we introduce the polycation poly(L-lysine) into the aqueous subphase. This leads to colored TPFs of similar quality to those corresponding to cationic surfactants (SI Appendix, Figure S21, Supporting Information), confirming that cations near the aqueous interface significantly accelerate TPF growth. It is important to note that WRAPPINGS differs fundamentally from earlier works that demonstrated the stabilization of colloid monolayers at the air–water interface by poly (cyanoacrylate) films,^[36–40] as well as the interfacial polymerization in heterogeneous systems (e.g., emulsions),^[41,42] which neither targeted nor achieved control over the film properties.

WRAPPINGS bears a resemblance to differences in reaction pathways, based on different alkyl substitutions, observed when CAs react with substances such as tertiary amines, which are known to promote adhesion between surfaces^[43,44] (SI Appendix, Supporting Information). Furthermore, our experiments reveal

Figure 1. Eco-friendly poly(cyanoacrylate) film synthesis at a surfactant-laden air–water interface using WRAPPINGS. a) Schematic of the experimental system. The essential components are an air–water interface containing cationic surfactant molecules (DTAB, marked blue) and ECA liquid monomer (super glue, marked red) in the upper panel. This system is practically realized by enclosing a sessile drop of aqueous DTAB solution in a culture dish that is covered with a lid carrying superglue droplets (bottom right). ECA monomers in the vapor phase (red spheres) polymerize upon contact with the air–water interface, forming PECA chains that create a film over the sessile DTAB droplet (bottom left). Inset: reflection micrograph of a PECA film on DTAB solution ($C_s = 2 \text{ mM}$) at $t_{\text{pol}} = 12 \text{ min}$ (Movie S1, Supporting Information). b) Reflection micrograph of a PBCA film. c) Photograph of a free-standing PECA film held by forceps. Both films (b, c) were grown on DTAB solution ($C_s = 3 \text{ mM}$, $t_{\text{pol}} = 40 \text{ min}$) and deposited on the substrate after water removal. d,e) SEM images of free-standing films grown on DTAB solutions. The top-view of a PECA film ($C_s = 0.5 \text{ mM}$, $t_{\text{pol}} = 120 \text{ min}$) shows a smooth surface (d), whereas the cross-section of a PBCA film (volume 3.5 mL, $C_s = 0.5 \text{ mM}$, $t_{\text{pol}} = 60 \text{ min}$) reveals its sub- μm thickness (e). f–k) Reflection micrographs of PECA films grown onto DTAB solutions ($C_s = 2 \text{ mM}$) for various t_{pol} and transferred onto Si wafers. Color results from thin-film interference are verified by simulations (insets), l) reflection microspectroscopy, and m) thickness measurements using atomic force microscopy. Scale bars are 1 cm (a, b, and c), 10 μm (d), 1 μm (e), and 100 μm (f–k).

that colored TPFs form on solutions of triethylamine (SI Appendix, Figure S22, Supporting Information) or sodium bicarbonate (SI Appendix, Figure S23, Supporting Information), both known to yield high molecular weight PCAs.^[44,45] Notably, a concentration of at least 1 mM is required for these substances to lead to qualitatively similar colored films, in stark contrast to the few μM needed with DTAB, illustrating a three-order magnitude higher concentration requirement. This significant difference arises because hydrophilic polycations, amines, and salts dissolve in the bulk aqueous phase, while surfactants accumulate at the surface. As a result, cationic surfactants ensure sufficient surface concentration at a much lower bulk concentration (SI Appendix, Supporting Information). The critical role of cationic surfactant is further emphasized by FTIR experiments indicating the presence of DTAB within the PECA films (SI Appendix, Figure S24, Supporting Information). We conjecture that the cationic heads form complexes with the growing polymer chains that make up the uniform TPF at the aqueous interface.

2.3. Tunable Planar Films: Programming Shape, Size, and Color

Using an air–water interface as a template for interfacial polymerization opens possibilities for manipulating the morphological features of TPFs. To illustrate this, we create a heart-shaped interface by confining a DTAB solution within a hydrophilic region patterned on a hydrophobic substrate using corona treatment. Upon exposure to ECA, a heart-shaped film with homogeneous azure color forms (Figure 2a, SI Appendix, Figure S25, Supporting Information). This film patterning approach can be extended to curved substrates if the solution volume is kept low enough for capillary forces to hold it in place. One example of such a conformal film is shown in Figure 2b; this silver PECA film in the shape of Luxembourg is formed on a ping-pong ball (SI Appendix, Figure S25, Supporting Information). The same approach is used in Figure 2c,d, SI Appendix, Figure S26 (Supporting Information) to make silvery films shaped like Z and O ($t_{\text{pol}} = 10$ min), but for the latter, we modify the color to orange after the end of the initial polymerization by re-exposing the film to ECA. An additional polymerization step initiated by moisture adsorbed on the film increases d_f to alter the interference color. In another example, we dry an E-shaped DTAB solution drop, driving surfactant deposition onto the substrate area defined by the pattern. We then fabricate an E-shaped PECA film by adding water onto the substrate and exposing the resulting solution to ECA (Figure 2e, SI Appendix, Figure S26, Supporting Information).

We can also manipulate the physical properties within a single PECA film by spatially modulating the polymerization kinetics. This is achieved by replacing DTAB with a photosensitive cationic surfactant, AzoTAB.^[46] AzoTAB is an azobenzene trimethyl ammonium bromide surfactant that undergoes an isomerization from a *trans*-rich state (CMC = 12.6 mM) to a more polar *cis*-rich state (CMC = 14.6 mM^[47]) upon UV irradiation at 365 nm (SI Appendix, Figure S27, Supporting Information). This photo-induced polarity change results in UV-induced depletion of surfactant at the interface,^[48] an increase in surface tension,^[49] and a decrease in cooperative electrostatic interactions with oppositely charged objects, including colloids^[50] and anionic polyelectrolytes.^[51] Thus, we hypothesized that shining

patterned UV light onto a drop exposed to ECA would enrich the non-irradiated area in cationic surfactants interacting more with ECA (here, *trans*-AzoTAB), and, therefore, locally accelerating the PECA growth. Figure 2f–h shows films transferred onto Si wafers with a patterned Minoan double axe, the mythical Griffin, and the Eiffel tower (SI Appendix, Movies S5 and S6, and Figure S28, Supporting Information). The color variation, from yellow for the irradiated area to turquoise for the dark area, confirms the greater d_f of the latter. These results confirm our proposed mechanism, where interfacial cations are instrumental in the TPF formation by modulating the chain growth. From a practical viewpoint, our approach allows us to prepare TPFs with programmable color patterns using an external stimulus that can be easily controlled in time and in space.

2.4. In Situ Packaging of Chemical and Biological Liquid Cargos

WRAPPINGS further expands into encapsulating aqueous liquids, a topic that has received increased attention recently.^[29,30] Here, we expose a pendant DTAB solution drop to ECA vapor, resulting in a PECA film on its surface. The accompanying decrease in air-drop interfacial tension results in a pear-like shape (Figure 3a). After an adequate t_{pol} to yield a mechanically robust polymer membrane, we stop the monomer supply and inject more liquid into the elastic liquid package. We then gently shake the partially encapsulated drop and place it on a substrate, ensuring that only the polymerized part touches it. Re-exposing the drop to ECA leads to polymerizing its bare part and a complete liquid enclosure with PECA. This results in a self-standing, dumpling-shaped encapsulated liquid package (Figure 3b). This liquid package can be easily manipulated and transported with a pair of tweezers (Figure 3c) or placed on different surfaces without sticking to them (SI Appendix, Movie S7 and Figure S29, Supporting Information). Compared to state-of-the-art methods for encasing macroscopic aqueous drops with polymer, WRAPPINGS eliminates the necessity of either organic solvents (of lower density than water) supporting a prefabricated TPF that encapsulates a drop falling on it,^[29] or a polymer dissolved in an organic solvent with specific properties (i.e., appropriate water miscibility and interfacial tension).^[30] Furthermore, liquid packages are fully wrapped by a TPF with tunable thickness, as opposed to liquid marbles, which are drops partially covered by solid particles.^[52]

WRAPPINGS may be further used to preserve (e.g., by slowing down drying) or protect (e.g., from contamination) aqueous samples by sealing them with a TPF. The softer polymer PBCA is used to encapsulate a large (≈ 200 μL) puddle, preventing the liquid from flowing when inclined (Figure 3d, Movie S8, Supporting Information). Significant liquid volumes (≈ 7.5 mL) can also be encapsulated by increasing d_f , so liquid cannot flow out of the dish even upon reversal (Figure 3e, SI Appendix, Movie S9, Supporting Information). To further highlight the liquid packaging robustness, we show an example of a drop coated with a TPF thick enough to be at the limit of minute permeability: we wrap a sessile drop containing methylene blue with a PBCA film, which keeps the drop intact upon immersion in water while preventing dye diffusion (Figure 3f). Conversely, the film permeability can be adjusted to have a finite value by changing d_f .

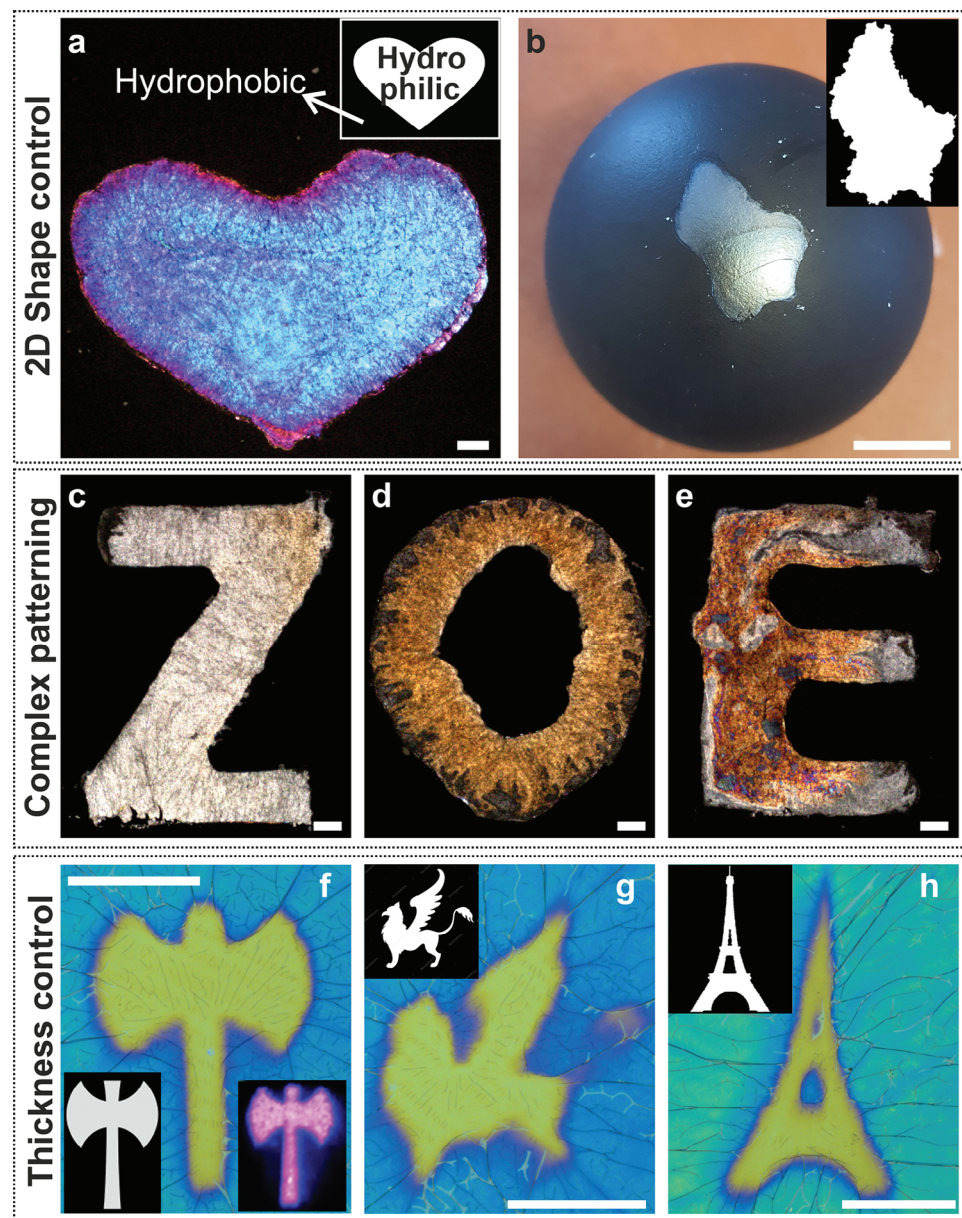


Figure 2. Thin PECA films with tailored size, shape, and color. Exposure of shaped DTAB solutions ($C_s = 2 \text{ mM}$, $40 \mu\text{L}$), created with wettability patterns, to ECA vapor yields a) a heart-shaped PECA film on a planar substrate ($t_{\text{pol}} = 20 \text{ min}$) or b) a curved PECA film, with the shape of Luxembourg, conforming to the supporting ping-pong ball ($t_{\text{pol}} = 5 \text{ min}$). c–e) Other strategies for preparing complex-shaped films (SI Appendix, Figure S25, Supporting Information). A Z-shaped DTAB solution ($C_s = 2 \text{ mM}$, $20 \mu\text{L}$) is exposed to ECA ($t_{\text{pol}} = 10 \text{ min}$), yielding a dry, silver-colored film (c). An O-shaped dry film is created the same way before being re-exposed to ECA vapor ($t_{\text{pol}} = 10 \text{ min}$), which leads to a color change from silver to orange (d). An E-shaped, multicolor film is created by water addition ($22 \mu\text{L}$) onto a pre-deposited DTAB pattern and exposure ($t_{\text{pol}} = 10 \text{ min}$) to ECA (e). f–h) Two-color films are created by irradiating drops of photosurfactant (AzoTAB) solutions ($C_s = 5 \text{ mM}$, $100 \mu\text{L}$) with structured UV light (wavelength 365 nm), simultaneously exposed to ECA ($t_{\text{pol}} = 25 \text{ min}$). The films are transferred onto Si wafers after the polymerization ends. Examples of PECA films with patterns of the Minoan double axe (f), mythical Griffon (g), and Eiffel tower (h). Insets: the photomasks used (f–h) and a UV pattern example (f). Scale bars are 1 mm (a), 1 cm (b), $100 \mu\text{m}$ (c–e), and 1 mm (f–h).

We show this by encapsulating a drop containing Rhodamine B with a comparatively thinner PBCA film. Upon drop immersion in phosphate-buffered saline solution, the dye progressively diffuses into the buffer, with half released over $\approx 50 \text{ h}$ (Figure 3g, SI Appendix, Figure S30 and Movie S10, Supporting Information). To our knowledge, these are the first demonstrations of the direct TPF syntheses onto aqueous specimens to encapsulate them. Re-

cent works (e.g., on initiated CVD for enclosing low vapor pressure organic liquids with polymer^[53] or plasma-induced polymerization at atmospheric pressure for encapsulating acrylate-based reactive liquids^[54]), although limited to organic liquids, highlight the potential of liquid packaging.

Notably, in Figure 3g–j, PBCA is synthesized utilizing a commercial product used for veterinarian surgery.^[55] This is

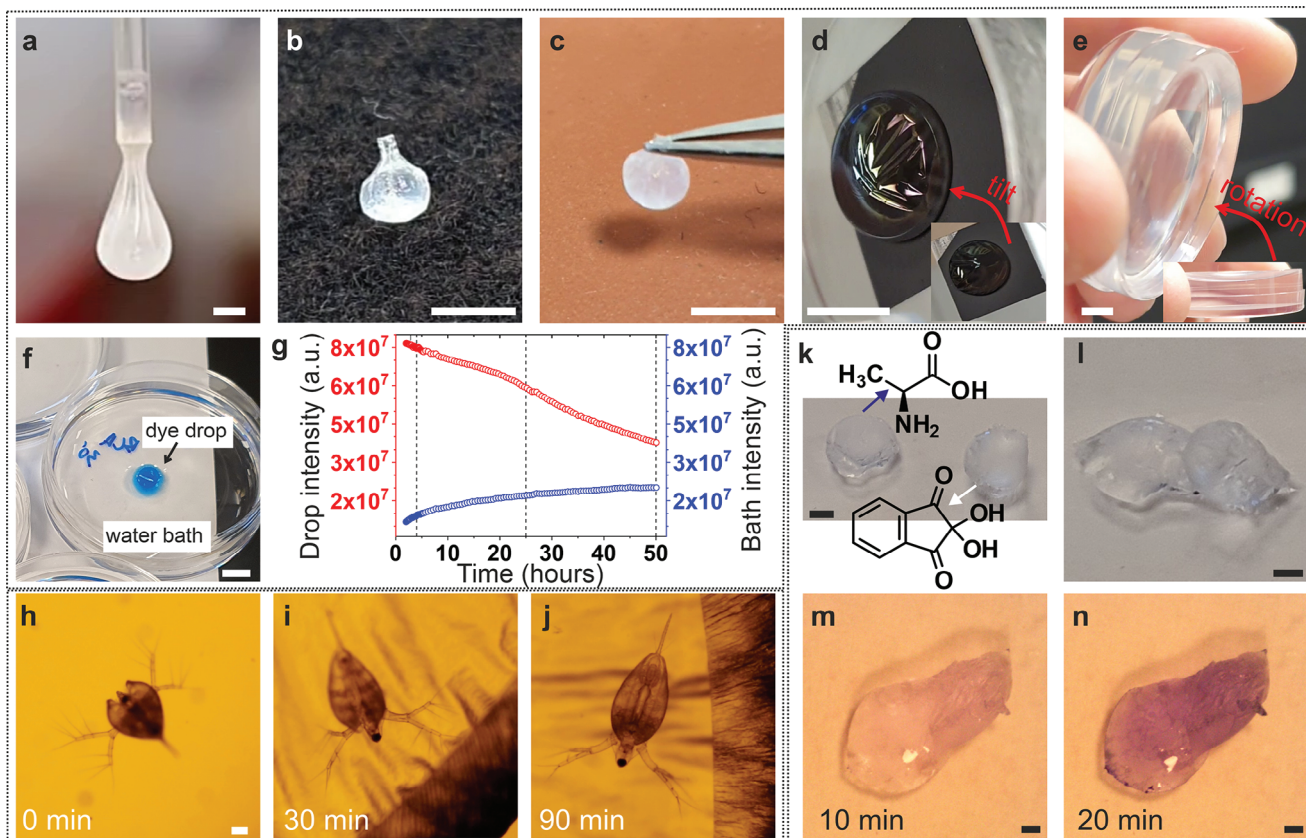


Figure 3. Encapsulation of aqueous chemical and biological cargos. a–c) The creation of free-standing liquid dumplings involves wrapping a DTAB solution pendant drop ($C_s = 0.2$ mM, ≈ 10 μ L) with PECA (a), followed by detaching the drop to completely polymerize it by re-exposing it to ECA (b). The liquid package can be manipulated with tweezers (c). d–f) Growing PBCA of varying thickness on large DTAB solution volumes can (d) immobilize a 200 μ L puddle ($C_s = 50$ μ M, $t_{\text{pol}} = 10$ min) on a tilted substrate (inset: sample position before tilting), (e) contain ≈ 7.5 mL of solution ($C_s = 0.2$ mM, $t_{\text{pol}} = 3$ h) in a dish even placed upside-down (inset: sample position before rotation), and (f) make a ≈ 10 μ L sessile drop (DTAB + methylene blue, $t_{\text{pol}} = 30$ min) withstand partial immersion in water, while preventing dye leaching. Conversely, d_r can be decreased ($t_{\text{pol}} = 2$ min) to allow dye release from a drop (10 μ L) of DTAB solution ($C_s = 0.5$ mM) and Rhodamine B into a phosphate-buffered saline solution. The release kinetics is followed in real-time by monitoring the fluorescent intensity of the drop and bath, respectively (g). h–j) In situ encapsulation of a drop ($C_s = 100$ μ M, 200 μ L) containing a Daphnia (h) with a biocompatible PBCA film. The swimming Daphnia is observed until the end of polymerization ($t_{\text{pol}} = 30$ min) (i) and even 60 min later (j). k–l) Following the method in (a–c), we form two PECA dumplings containing alanine and ninhydrin (both 1 wt%) and DTAB ($C_s = 0.2$ mM, (k). Real-time monitoring of the aminoacid-indicator reaction gradually turns the initially transparent liquid into purple upon squeezing the dumplings against each other (l). m,n) The time after mixing is indicated. Scale bars are 1 mm (a), 5 mm (b–f), 100 μ m (h–j), and 1 mm (k–n).

because PBCA has low toxicity and is biodegradable, making WRAPPINGS an ideal strategy for the non-invasive, in situ encapsulation of living organisms.^[42] To demonstrate this, we expose a drop containing a small planktonic crustacean, Daphnia, to BCA (SI Appendix). Water contains DTAB at $C_s = 100$ μ M that is low enough not to harm Daphnia, nonetheless adequate to accelerate TPF growth (Figure 3h, SI Appendix, Movie S11, Supporting Information). The transparent PBCA allows us to observe that the swimming behavior of Daphnia remains unaltered during polymerization (Figure 3i, Movie S11, Supporting Information), and for over 60 min after the polymerization (Figure 3j, Movie S11, Supporting Information).

The capability of PCA films to confine aqueous liquids into self-standing objects (Figure 3a–c) opens numerous possibilities for facile microfluidic operations. This is demonstrated by creating two self-standing drops containing alanine and ninhydrin, respectively (Figure 3k). Ninhydrin is an indicator used to detect amino acids like alanine, and their reaction produces a

chromophore called Ruhemann's purple.^[56] By bringing the two packages into contact through gentle pressure, the liquids mix through diffusion (Figure 3l), enabling the reaction that progressively turns the initially clear mixture to purple (Figure 3m,n, SI Appendix, Movie S12, Supporting Information). The optical clarity of the film allows observation by the unaided eye, thus following the reaction evolution in real time without any equipment. The developed packaged liquids have attractive properties similar to liquid marbles^[52] (e.g., non-sticking nature, transparency) without the constraint of utilizing nanoparticles with specific wettability^[57] or size.^[58]

2.5. In Situ Gas Encapsulation and Manipulation with Solid Bubbles

We next show that WRAPPINGS can also be used to encapsulate and manipulate gaseous samples in situ. Previous studies

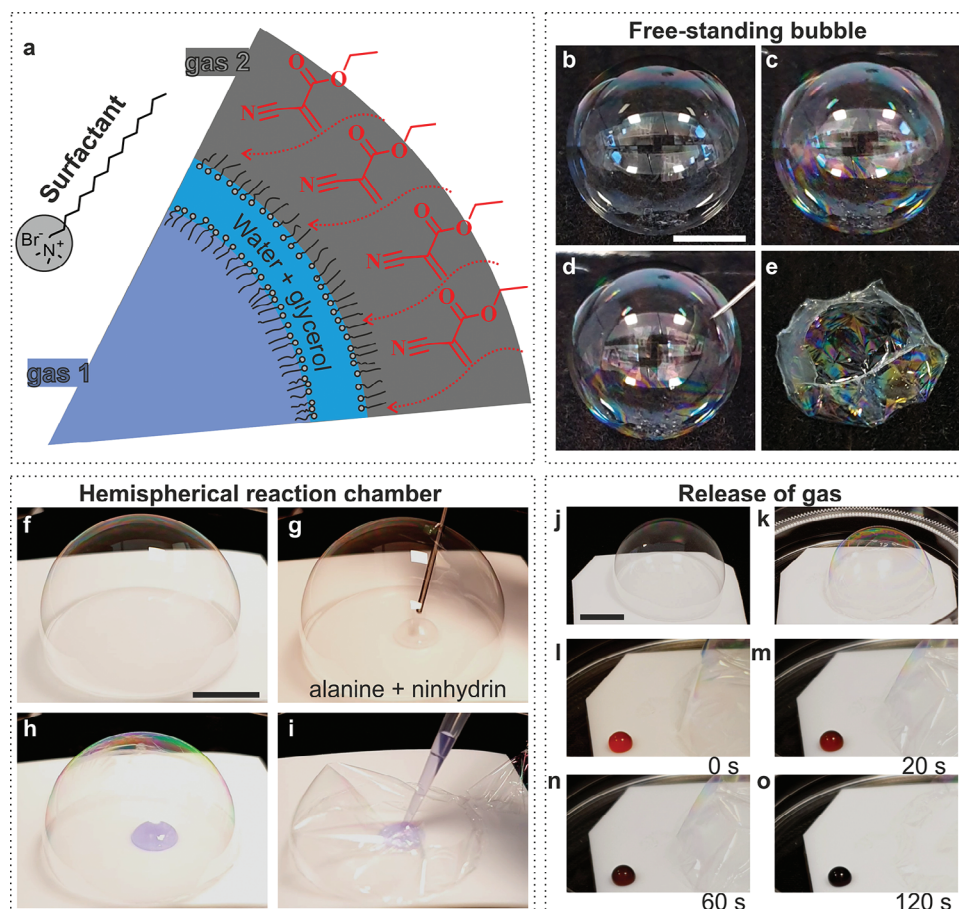


Figure 4. Encapsulating and handling gaseous specimens. a) Schematic of a soap bubble comprising a film of CTAB and glycerol solution that is solidified by ECA introduced in the outer gas. b–e) A quasi-spherical air bubble (≈ 5 mL) enclosed by ≈ 10 μ L of CTAB ($C_s = 6$ mM) and glycerol (20 wt%) aqueous solution is created (b) and polymerized by ECA vapor diffusing through the supporting cloth for $t_{\text{pol}} = 10$ min (c). Piercing with a needle (d) results in a colorful, elastic film collapsing onto the fabric (e). f–i) We form a PECA reaction chamber by first making a hemispherical bubble (6 mL) with an aqueous solution of CTAB ($C_s = 5.95$ mM) and glycerol (30 wt%) on a PTFE substrate (f), in which we dispense two drops containing alanine (1.05 wt%) and ninhydrin (1.04 wt%) using a needle prewetted with bubble solution (g). The transparent PECA chamber ($t_{\text{pol}} = 10.5$ min) allows the (h) real-time monitoring of the aminoacid-indicator reaction progress via the color change in the drop and (i) collecting the reaction product. j–o) After making a sessile bubble containing 8 mL of air saturated with acetic acid using a solution of CTAB ($C_s = 5.94$ mM) and glycerol (20.1 wt%) on a PTFE substrate placed in a dish (j), we polymerize it for $t_{\text{pol}} = 10$ min (k). We then dispense a drop containing Congo Red (0.04 wt%) next to it. At $t = 0$, the gas is released by breaking the bubble (l), whereafter, it gradually diffuses into the drop to lower its pH, leading to a progressive color change from red to black (m–o). All scale bars are 1 cm.

have shown that gas encapsulation is achievable in the microscale (≈ 1 – 20 μ m) by the layer-by-layer assembly of polyelectrolytes onto microemulsion bubbles.^[59] Our conceptually different strategy utilizes soap bubbles, thin films of water and glycerol stabilized by surfactants (Figure 4a). In the first example, we create a spherical bubble by injecting air into a tip containing soap bubble solution. We then detach the bubble by gently shaking it and placing it on a fabric (Figure 4b). The resulting quasi-spherical bubble is polymerized by passing ECA vapor through the fabric, yielding a PECA film on its outer surface (Figure 4c, SI Appendix, Figure S31 and Movie S13, Supporting Information). We can destabilize the bubble by piercing it with a sharp object (Figure 4d, SI Appendix, Movie S14, Supporting Information), which results in a collapsed, elastic TPF with vivid colors (Figure 4e). Although quasi-spherical, polymerized bubbles can remain stable for several months (SI Appendix, Figure S32, Supporting Information),

it is challenging to maintain a freshly created bubble during an adequate polymerization time leading to a robust TPF. To tackle this challenge, we use a partially wetting substrate to generate a hemispherical bubble that shows superior stability against popping (Figure 4f). Upon ECA exposure, the outer surface of the bubble is polymerized, creating a dome-shaped elastic film (SI Appendix, Figure S33, Supporting Information). This geometry allows the dispensing of ninhydrin and alanine solution drops (Figure 4g, Movie S15, Supporting Information). We take advantage of the self-healing nature of soap films, their ability to respond rapidly to mechanical disturbances and repair themselves efficiently,^[60] and dispense ninhydrin and alanine solution drops (Movie S15, Supporting Information). This is done by utilizing a needle prewetted with the same solution used to make the bubble, ensuring the bubble remains stable after retracting the needle. Subsequent polymerization with ECA vapors transforms the

bubble into a solid reactor (Movie S15, Supporting Information). Its transparency allows for visual monitoring of the occurring reaction, as evidenced by the drop turning purple (Figure 4h, SI Appendix, Figure S34, Supporting Information). The reaction product can also be collected by cutting the chamber with a scalpel (Figure 4i, SI Appendix, Movie S15, Supporting Information).

Solid bubbles can also incorporate reactive gases that participate in a chemical reaction. To show this, we form a solid bubble that contains acetic acid mixed with air (Figure 4j,k, Movie S16, Supporting Information) next to a solution drop of Congo Red, a pH-sensitive dye. The drop remains red, indicating that the enclosed gas is contained within the bubble (Movie S16, Supporting Information). The gas-dye reaction is initiated by breaking the bubble (Figure 4l), which allows the acidic gas to diffuse away. This causes the drop to gradually turn dark red and eventually black (Figure 4m–o). Other gases, such as inert CO₂ or more reactive gases like triethylamine, can also be enclosed (SI Appendix, Figure S35, Supporting Information). To the best of our knowledge, we are not aware of reported polymerization mechanisms and materials that could combine all the features in a single method as in WRAPPINGS.

3. Conclusion

WRAPPINGS is a novel concept yielding biocompatible TPFs with customizable microscopic and macroscopic properties that relies on the polymerization of superglues on aqueous interfaces containing interfacial cationic species (e.g., surfactants, polyelectrolytes). The simplicity of this concept is demonstrated by the capability to prepare thin PCA films even at home, using materials used in everyday life, without requiring specialized equipment (SI Appendix, Figure S36 and Movie S17, Supporting Information). This results in a modular platform with unique outcomes, including complex TPFs with spatially or temporally controlled thickness and interference color (SI Appendix, Figure S37, Supporting Information). Additionally, WRAPPINGS allows in situ encapsulation of various aqueous and gaseous specimens, including living organisms as well as reactive and inert chemicals. The ability to customize the PCA chemistry^[61] and thickness potentially allows for the programmable release of drugs, liquids, and gases into physiological or other environments,^[62] as well as the stabilization of fluid interfaces for robust heterogeneous systems^[41] and self-standing liquids without using specifically engineered nanoparticles.^[52] These aspects make WRAPPINGS a powerful yet eco-friendly platform for several demanding operations. Fundamentally, the action of cationic species as stabilizing accelerators enables the exploration of analogous effects in other systems. We hope our study will act as a seed for further innovation by scientists and engineers across multiple disciplines.

4. Experimental Section

The WRAPPINGS concept involves the exposure of the surface of an aqueous solution containing cationic species that act as stabilizing accelerators for the polymerization of cyanoacrylate monomer. Hence, there are three key ingredients: water, a cationic substance, and a monomer. The performance of various substances, both laboratory-grade and commercial products used in everyday life, as core ingredients for WRAPPINGS

was tested. For more information on those, as well as all other materials used for the film synthesis and encapsulation experiments (e.g., salts, dyes, Daphnia, gases), and the experimental setup (e.g., substrates, sample cells, polymerization chambers), see the Supporting Information.

TPF Generation: In a typical experiment, as illustrated schematically in Figure 1, an aqueous surfactant solution was placed inside a chamber in which polymerization occurs. The solution may be either in the form of a sessile drop or a larger liquid puddle deposited on a solid substrate, a large liquid volume held within a black plastic lid, a pendant drop, or a quasi-spherical or sessile bubble resting on a substrate. The reaction chamber may be either a culture dish or a jar (see Supporting Information). In any case, the desired number of monomer drops is dispensed on the top (or bottom) surface of the reaction chamber. A positive displacement pipette (Multipette M4, Eppendorf, Germany) was used to i) make monomer drops of precise volume (typically 4 μ L each) and ii) ensure that the pipette was not contaminated by polymer forming on any surface containing water moisture. The reaction chamber was closed with a lid immediately after the monomer drops were placed on it; this was the onset of the polymerization ($t_{\text{pol}} = 0$). The polymerization was started rapidly; this was based on the high volatility of the cyanoacrylates used: the boiling points of ECA, ICA, and BCA were 54 °C (at 0.21 kPa), 53 °C (at 0.27 kPa), and 83 °C (at 0.40 kPa), respectively.^[27] Experiments generating planar TPFs were performed in an incubator with a controlled temperature (25 °C). The ambient relative humidity was typically in the \approx 38–64% range; note that qualitative differences in film formation within this range was not observed.

Isolation of TPFs from the Air–Water Interface: Thin PECA films formed on the free surface of drops may be deposited onto the supporting solid substrate by removing all water (and almost all surfactant) under the film. This was achieved by combining the usage of paper tissue, enabling most of the solution to be drained via capillary forces and evaporation that removes the remaining water (Movie S2, Supporting Information). Dry deposited films may be lifted from the substrate (Movie S3, Supporting Information) and transferred to another substrate. Alternatively, TPFs formed either on the surface of water puddles (including photopatterned films) or on larger volumes of water contained within lids may be transferred onto solid substrates using another procedure involving floating the films on a large volume of ultrapure water. This enabled the complete removal of surfactants while reducing film wrinkling (Movies S4 and S5, Supporting Information).

Generation of Planar TPFs of Arbitrary Shape and Size: To create a planar or curved film of arbitrary shape and size, the free interface of the surfactant solution was shaped by placing it on a substrate having a wettability pattern. A flat or curved substrate was started, first coated with a material based on silicone resin (see Supporting Information), which renders the substrate black and hydrophobic. Next, the desired pattern on a paper sticker was placed (SI Appendix, Figure S25a,e, Supporting Information) on the hydrophobic substrate. A corona plasma treater (Corona SB, BlackHole Lab) was used to make the unprotected surface of the substrate hydrophilic. After removing the sticker, a wettability pattern was created comprising a hydrophilic area surrounded by a hydrophobic one. Dispensing the appropriate volume of surfactant solution on the hydrophilic part led to a free interface of the desired size and shape (SI Appendix, Figure S25b, Supporting Information). Cyanoacrylate polymerization on this shaped interface was conducted as described above, leading to shaped TPFs (SI Appendix, Figure S25c,d, f–i, Supporting Information).

Generation of Liquid Dumplings: Apart from planar interfaces, any aqueous entity, regardless of its shape, may be used as a template for growing PCA films. To demonstrate the potential of WRAPPINGS for packaging liquids, a pendant DTAB solution drop (volume on the order of \approx 10 μ L) was formed using a 1 mL plastic syringe (Injekt F, Braun) and a PTFE needle with 1 mm diameter (KRÜSS GmbH, Germany). The pendant drop was then exposed to ECA vapor, which led to a thin PECA film covering its surface. Once a sufficient t_{pol} had passed to yield a mechanically robust polymer membrane, the monomer supply was stopped. Then more liquid was injected into the elastic micro-balloon to increase its weight. By gently shaking the needle, the partially encapsulated drop was detached and it was placed on a solid substrate, ensuring that only the polymerized

part of the drop encounters the substrate. Subsequently, the drop once again was exposed to ECA vapor to polymerize the bare part of it, hence, the liquid was fully enclosed with PECA. All liquid dumping experiments were conducted in ambient temperature ($\approx 22\text{--}24\text{ }^\circ\text{C}$) and relative humidity ($\approx 38\text{--}64\%$) conditions.

Generation and Solidification of Soap Bubbles: A soap bubble, a thin liquid film stabilized by a bilayer of surfactants, constituted an ideal platform for handling gases while including the key components required to form a TPF using WRAPPINGS. From a practical perspective, to polymerize a soap bubble using this concept, it was imperative to prepare long-lasting bubbles, i.e., with a lifetime of at least several minutes. Although various recipes for making long-lasting soap bubbles are available, they typically rely on commercial dishwashing liquids (see ref. [63] and references therein). Apart from containing numerous substances at unknown concentrations, commercial formulations contain mostly anionic surfactants; this was incompatible with WRAPPINGS, necessitating the use of cationic species. For these reasons, aqueous solutions (which are called bubble solutions) were developed to yield bubbles that remained stable long enough for WRAPPINGS to be efficient in solidifying them (i.e., on the order of ≈ 5 min). The bubble solutions were prepared by adding in a vial, in this order, the appropriate amount of ultrapure water, concentrated aqueous CTAB solution, and glycerol; different formulations were tested, and the exact concentrations of each substance were given in the figure corresponding to each experiment reported here. Typically, these samples were mixed gently by hand (to avoid forming bubbles) and then heated to $\approx 50\text{ }^\circ\text{C}$ for a few minutes to achieve homogenization. The homogeneous bubble solutions were kept in an orbital mixer for an additional ≈ 2 h.

Two different bubble geometries were explored. First, a spherical soap bubble was formed using either a 10 or a 20 mL plastic syringe (Injekt, Braun) with an attached rubber tube connected to a plastic micropipette tip (Eppendorf). Air was injected into the micropipette tip that contained a small volume (typically on the order of $\approx 10\text{ }\mu\text{L}$) of the bubble solution. By gently shaking the tip, the bubble was detached and it was deposited as a quasi-spherical, self-standing object on a fabric. Next, ECA vapor was passed through the porous fabric, and the quasi-spherical bubble was solidified as a PECA film forms on its outer surface. Second, using the same setup and procedure described above, initially a small spherical bubble was created, which was brought in contact with a partially wetting substrate. Upon touching the solid surface, it became a sessile bubble with a dome shape. The size of the sessile bubble could be adjusted by injecting additional air into it. Sessile bubbles were polymerized following the procedure used for sessile drops of surfactant solutions. All bubble polymerization experiments were conducted in ambient temperature ($\approx 22\text{--}24\text{ }^\circ\text{C}$) and relative humidity ($\approx 38\text{--}64\%$) conditions.

Photopatterning Setup for Making PECA Films with Two-Color Patterns: A home-built optical setup irradiated sessile drops of aqueous AzoTAB solution that were exposed to ECA vapors (SI Appendix, Figure S27, Supporting Information). UV light (wavelength 365 nm) from an LED source (CoolLED pE-300 White) was delivered to an inverted fluorescence microscope (Ti2-U Eclipse, Nikon) by means of a liquid light guide (CoolLED). Photomasks were prepared by printing the desired pattern twice on transparent plastic foils with a printer. The photomasks were cut in the size and shape of optical filters and were inserted in the light path. The resulting light pattern was focused on the free surface of the sessile drop using a microscope objective (10 \times , Nikon). The drop was dispensed on a poly(styrene) substrate (culture dish lid, diameter 38 mm), itself placed in a culture dish (diameter 100 mm, volume $\approx 173\text{ cm}^3$); the latter was covered with a lid, onto which 8 drops (4 μL each) of ECA (commercial superglue) were dispensed. All photopatterning experiments were conducted in a temperature range of $\approx 22\text{--}23\text{ }^\circ\text{C}$ and a relative humidity range of $\approx 38\text{--}64\%$.

Modeling of Thin Film Interference Colors: The principles of thin film interference were used to calculate the refractive index of the film and model the colors of reflected light.^[64] The model consisted of 3 layers: an air layer with a refractive index, $n_a = 1$, a thin film of unknown refractive index, n_f and thickness, d_f , and a SiO_2 substrate, n_{SiO_2} (SI Appendix, Figure S13, Supporting Information). The SiO_2 substrate used had a thickness of 650 μm and was considered infinite in the model. The refractive index of

SiO_2 was considered as constant with the value of $n_{\text{SiO}_2} = 1.465$ ^[65] and assumed a normal incidence angle.

To determine the refractive index of the film, the experimental reflectance spectra of films and corresponding thicknesses, d_f , measured using AFM were analyzed. Initially, the positions of transmittance minima and maxima in the spectra were identified, which indicated constructive or destructive interference and were linked to the phase shifts of the reflected waves. For the assumption $n_a \langle n_f \rangle n_{\text{SiO}_2}$ the constructive

$$2n_f d_f = m\lambda, m = 0.5, 1.5, 2.5, \dots \quad (1)$$

and destructive

$$2n_f d_f = m\lambda, m = 0, 1, 2, \dots \quad (2)$$

interference conditions were obtained, respectively. The range of wavelengths between 410 and 720 nm was analyzed to identify the peaks correctly. To achieve this, the measurement noise was filtered out and the spectra were smoothed curves using the moving average of 85 data points. Using this method, the peaks of 39 different reflectance spectra of films with nine different thicknesses were identified (SI Appendix, Figure S14a, Supporting Information). Then a plot was created which displayed the wavelength at which each of the extrema (minima or maxima) occurred against the film thickness (SI Appendix, Figure S14b, Supporting Information). By applying Equation (1) and Equation (2), extrema with the same values of m were positioned along the line with the same slope, which was used to determine m for each extremum.

After m for each extremum was identified, the relation $\frac{m\lambda}{2} = n_f d_f$ was used, following Equation (1) and Equation (2), to determine the refractive index of the film from the slope of the plot. The result is shown in SI Appendix, Figure S15 (Supporting Information). The calculated value of the refractive index of the film was $n_f = 1.505 \pm 0.022$, and the R-squared value of the fit was above 0.98. Note that the possible error in the thickness measurement was taken into account during the calculation.

Once the refractive index of the film was known, the reflectivity of the system could be calculated using the Fresnel equations. The reflection coefficient of light passing through a boundary between two layers with different refractive indices was calculated as

$$r = \frac{n_1 - n_2}{n_1 + n_2} \quad (3)$$

while the transmission coefficient was calculated as

$$t = \frac{2n_1}{n_1 + n_2} \quad (4)$$

where the light propagated from a medium with n_1 into a medium with n_2 (3).

The spectral intensity of light S_{ref} reflected from the system, which consisted of 3 layers, was calculated as

$$S_{\text{ref}}(\lambda) = (A^2 + B^2 + 2AB\cos(\phi_B(\lambda) - \phi_A)) S_{\text{in}}(\lambda) = C_{\text{ref}}(\lambda) S_{\text{in}}(\lambda) \quad (5)$$

where the spectral intensity of the incoming light (i.e., illumination) $S_{\text{in}}(\lambda)$, which was measured in the experiment, was multiplied by the coefficient $S_{\text{in}}(\lambda)$ that took into account the interference between first and second-order reflections as described in the following and shown in SI Appendix, Figure S14 (Supporting Information). The interference coefficient $C_{\text{ref}}(\lambda)$ was calculated from the sum of the two reflected waves, where $A = \left| \frac{n_a - n_f}{n_a + n_f} \right|$ is the ratio between the amplitude of the incoming light and the light that is reflected from the first boundary (between air and the film) and $B = \frac{2n_a}{n_a + n_f} \frac{n_f - n_{\text{SiO}_2}}{n_f + n_{\text{SiO}_2}} \frac{2n_f}{n_a + n_f}$ is the ratio between the amplitude of the incoming light and the light that is transmitted through the first boundary (between air and the film), reflected from the second boundary (between film and SiO_2), and transmitted through the first boundary again. $\phi_A = \pi$ is

the phase that is acquired by the first wave when reflected from the first boundary and equals to π , as $n_f > n_a$.

$\phi_B = 4\pi n_f d_f \lambda$ is the phase that is acquired by the wave with the amplitude B when passing through the film with the thickness d_f , being reflected from the second boundary and passing through the film again. No additional phase was acquired during reflection from the second boundary, as $n_{\text{SiO}_2} < n_f$. Higher-order reflections and material refractive index dispersion were both neglected. The spectral intensity, which depended on the refractive index and the thickness of the film, was calculated by Equation (3) and then transformed into an RGB picture using the same color functions and white balance values as in the Pixelink capture OEM software, used to generate experimental pictures. The resultant TPF color spectrum was shown in SI Appendix, Figure S16 (Supporting Information).

Supporting Information

Supporting Information is available from the Wiley Online Library or from the author.

Acknowledgements

The authors are indebted to Jacopo Vialetto for early-stage film characterization experiments and Athena Anastasaki, Richard Whitfield, and Nghia Truong Phuoc for experiments and fruitful discussions on poly(cyanoacrylate) characterization. They thank Martin Dulle for X-ray scattering experiments, Georgios Kordogiannis and Nikola Novak for DSC experiments, and Monique Wiesinger for technical support and several inspiring suggestions. They also thank Rijeesh Kizhakidathazhath, Maria Vamvakaki, Eleni Pavlopoulou, Emmanuel Stiakakis, Roberto Quintana, Mohan Srinivasarao, Syuji Fujii, Daniel Schmidt, and Damjana Drobne for fruitful exchanges at various stages of this research, and Igor Mušević and Albert Schenning for critically reviewing the manuscript. V.S.R.J. is grateful to Igor Mušević and Matjaž Humar for allowing access to their laboratories and acknowledges valuable discussions with Polona Umek.

Conflict of Interest

The authors declare no conflict of interest.

Data Availability Statement

The data that support the findings of this study are available in the supplementary material of this article.

Keywords

biodegradable polymers, fluid encapsulation, interfacial polymerization, poly(cyanoacrylate), superglue, thin films

Received: June 10, 2024

Revised: August 2, 2024

Published online:

[1] B. Li, S. Zhang, J. S. Andre, Z. Chen, *Prog. Polym. Sci.* **2021**, *120*, 101431.

[2] A. Khlustova, Y. Cheng, R. Yang, *J. Mater. Chem. B* **2020**, *8*, 6588.

[3] I. Vilaró, J. L. Yagüe, S. Borrós, *ACS Appl. Mater. Interfaces* **2017**, *9*, 1057.

[4] D. Soto, A. Ugur, T. A. Farnham, K. K. Gleason, K. K. Varanasi, *Adv. Funct. Mater.* **2018**, *28*, 1707355.

[5] T. L. Andrew, L. Zhang, N. Cheng, M. Baima, J. J. Kim, L. Allison, S. Hoxie, *Acc. Chem. Res.* **2018**, *51*, 850.

[6] D. B. Hall, P. Underhill, J. M. Torkelson, *Polym. Eng. Sci.* **1998**, *38*, 2039.

[7] E. Bindini, G. Naudin, M. Faustini, D. Grosso, C. Boissière, *J. Phys. Chem. C* **2017**, *121*, 14572.

[8] J. J. Richardson, M. Björnalm, F. Caruso, *Science* **2015**, *348*, 2491.

[9] K. K. Gleason, *Nat Rev Phys* **2020**, *2*, 347.

[10] D. Merche, N. Vandencastele, F. Reniers, *Thin Solid Films* **2012**, *520*, 4219.

[11] U. Czuba, R. Quintana, M. C. De Pauw-Gillet, M. Bourguignon, M. Moreno-Couranjo, M. Alexandre, C. Detrembleur, P. Choquet, *Adv. Healthcare Mater.* **2018**, *7*, 1701059.

[12] Y. Barkan, M. Levinman, I. Veprinsky-zuzuliya, T. Tsach, E. Merqioul, G. Blum, A. J. Domb, A. Basu, *Acta Biomater.* **2017**, *48*, 390.

[13] A. J. Singer, J. V. Quinn, J. E. Hollander, *Am. J. Emerg. Med.* **2008**, *26*, 490.

[14] I. S. Bayer, *Smart Nanoparticles for Biomedicine*, Elsevier Inc., **2018**.

[15] S. P. Wargacki, L. A. Lewis, M. D. Dadmun, *J. Forensic Sci.* **2007**, *52*, 1057.

[16] M. T. Masood, M. Zahid, L. Goldoni, L. Ceseracciu, A. Athanassiou, I. S. Bayer, *ACS Appl. Mater. Interfaces* **2018**, *10*, 34573.

[17] H. W. Coover, D. W. Dreifus, J. T. O'Connor, *Handbook of Adhesives*, Van Nostrand Reinhold, New York **1990**.

[18] E. Mele, J. A. Heredia-Guerrero, I. S. Bayer, G. Ciofani, G. G. Genchi, L. Ceseracciu, A. Davis, E. L. Papadopoulou, M. J. Barthel, L. Marini, R. Ruffilli, A. Athanassiou, *Sci. Rep.* **2015**, *5*, 14019.

[19] L. Zhang, N. Zhao, X. Li, Y. Long, X. Zhang, J. Xu, *Soft Matter* **2011**, *7*, 4050.

[20] A. J. Christy, S. T. Phillips, *Sci. Adv.* **2023**, *9*, 2295.

[21] Y. Cui, J. Chai, H. Du, Y. Duan, G. Xie, Z. Liu, G. Cui, *ACS Appl. Mater. Interfaces* **2017**, *9*, 8737.

[22] J. M. Korde, B. Kandasubramanian, *Biomater. Sci.* **2018**, *6*, 1691.

[23] C. Vauthier, *Polymer Nanoparticles for Nanomedicines*, Springer International Publishing, Cham **2016**.

[24] P. Couvreur, B. Kante, M. Roland, P. Guiot, P. BAuduin, P. Speiser, *J. Pharm. Pharmacol.* **1979**, *31*, 331.

[25] N. Al Khouri Fallouh, L. Roblot-Treupel, H. Fessi, J. P. Devissaguet, F. Puisieux, *Int. J. Pharm.* **1986**, *28*, 125.

[26] C. Vauthier, C. Dubernet, E. Fattal, H. Pinto-Alphandary, P. Couvreur, *Adv. Drug Delivery Rev.* **2003**, *55*, 519.

[27] P. Klemarczyk, *Adhesion Science and Engineering*, **2002**, Elsevier, p. 847.

[28] R. Sáez, C. McArdle, F. Salhi, J. Marquet, R. M. Sebastián, *Chem. Sci.* **2019**, *10*, 3295.

[29] D. Kumar, J. D. Paulsen, T. P. Russell, N. Menon, *Science (80-)*. **2018**, *359*, 775.

[30] S. Coppola, G. Nasti, V. Vespini, L. Mecozzi, R. Castaldo, G. Gentile, M. Ventre, P. A. Netti, P. Ferraro, *Sci. Adv.* **2019**, *5*, 5189.

[31] K. Xiong, G. Emilsson, A. Maziz, X. Yang, L. Shao, E. W. H. Jager, A. B. Dahlin, *Adv. Mater.* **2016**, *28*, 9956.

[32] M. Anyfantakis, Z. Geng, M. Morel, S. Rudiuk, D. Baigl, *Langmuir* **2015**, *31*, 4113.

[33] D. C. Pepper, *Makromol. Chemie. Macromol. Symp.* **1992**, *60*, 267.

[34] X. Zhang, X. Tang, K. Bowen, *Chem. Phys. Lett.* **2013**, *582*, 21.

[35] J. Huang, M. Juszkiewicz, W. H. de Jeu, E. Cerda, T. Errick, N. Menon, T. P. Russell, *Science (80-)*. **2007**, *317*, 650.

[36] N. Vogel, L. De Viguerie, U. Jonas, C. K. Weiss, K. Landfester, *Adv. Funct. Mater.* **2011**, *21*, 3064.

[37] N. Vogel, J. Ally, K. Bley, M. Kappl, K. Landfester, C. K. Weiss, *Nanoscale* **2014**, *6*, 6879.

[38] T. Sekido, S. Wooh, R. Fuchs, M. Kappl, Y. Nakamura, H. J. Butt, S. Fujii, *Langmuir* **2017**, *33*, 1995.

- [39] S. Fujii, E. Mouri, K. Akiyama, S. Nakayama, K. Uda, Y. Nakamura, H. Matsuoka, *Langmuir* **2017**, *33*, 1451.
- [40] J. Fujiwara, F. Geyer, H. Butt, T. Hirai, Y. Nakamura, S. Fujii, *Adv. Mater. Interfaces* **2020**, *7*, 2001573.
- [41] X. Lian, S. Liao, X. Q. Xu, S. Zhang, Y. Wang, *Macromolecules* **2021**, *54*, 10279.
- [42] J. Nicolas, P. Couvreur, *Wiley Interdiscip. Rev. Nanomed. Nanobiotechnol.* **2009**, *1*, 111.
- [43] Y. Okamoto, P. T. Klemarczyk, *J. Adhes.* **1993**, *40*, 81.
- [44] P. Klemarczyk, *Polymer (Guildf)* **2001**, *42*, 2837.
- [45] D. H. Park, S. B. Kim, K. D. Ahn, E. Y. Kim, Y. J. Kim, D. K. Han, *J. Appl. Polym. Sci.* **2003**, *89*, 3272.
- [46] A. Diguët, R.-M. Guillermic, N. Magome, A. Saint-Jalmes, Y. Chen, K. Yoshikawa, D. Baigl, *Angew. Chem., Int. Ed.* **2009**, *48*, 9281.
- [47] A. Diguët, N. K. Mani, M. Geoffroy, M. Sollogoub, D. Baigl, *Chem. - A Eur. J.* **2010**, *16*, 11890.
- [48] J. Vialetto, M. Anyfantakis, S. Rudiuk, M. Morel, D. Baigl, *Angew. Chem. Int. Ed.* **2019**, *58*, 9145.
- [49] N. Kavokine, M. Anyfantakis, M. Morel, S. Rudiuk, T. Bickel, D. Baigl, *Angew. Chem., Int. Ed.* **2016**, *55*, 11183.
- [50] M. Anyfantakis, D. Baigl, *Angew. Chem., Int. Ed.* **2014**, *53*, 14077.
- [51] A. Estévez-Torres, C. Crozatier, A. Diguët, T. Hara, H. Saito, K. Yoshikawa, D. Baigl, *Proc. Natl. Acad. Sci. U. S. A.* **2009**, *106*, 12219.
- [52] P. Aussillous, D. Quéré, *Nature* **2001**, *411*, 924.
- [53] M. M. De Luna, P. Karandikar, M. Gupta, *Mol. Syst. Des. Eng* **2020**, *5*, 15.
- [54] F. Rezaei, M. D. Dickey, P. J. Hauser, *J. Appl. Polym. Sci.* **2020**, *137*, 6.
- [55] F. Ollivier, M. Delverdier, A. Regnier, *Vet. Ophthalmol.* **2001**, *4*, 261.
- [56] D. J. McCaldin, *Chem. Rev.* **1960**, *60*, 39.
- [57] D. Zang, Z. Chen, Y. Zhang, K. Lin, X. Geng, B. P. Binks, *Soft Matter* **2013**, *9*, 5067.
- [58] M. Anyfantakis, V. S. R. Jampani, R. Kizhakidathazhath, B. P. Binks, J. P. F. Lagerwall, *Angew. Chem.* **2020**, *132*, 19422.
- [59] D. G. Shchukin, K. Köhler, H. Möhwald, G. B. Sukhorukov, *Angew. Chem., Int. Ed.* **2005**, *44*, 3310.
- [60] L. Courbin, H. A. Stone, *Phys. Fluids* **2006**, *18*, 10.
- [61] C. Gross-Heitfeld, J. Linders, R. Appel, F. Selbach, C. Mayer, *J. Phys. Chem. B* **2014**, *118*, 4932.
- [62] Z. Sheng, H. Wang, Y. Tang, M. Wang, L. Huang, L. Min, H. Meng, S. Chen, L. Jiang, X. Hou, *Sci. Adv.* **2018**, *4*, 6724.
- [63] S. Frazier, X. Jiang, J. C. Burton, *Phys. Rev. Fluids* **2020**, *5*, 013304.
- [64] O. Stenzel, *The Physics of Thin Film Optical Spectra*, Springer International Publishing, Cham **2016**.
- [65] S. Chongsawangvirod, E. A. Irene, A. Kalnitsky, S. P. Tay, J. P. Ellul, *Proc. - Electrochem. Soc.* **1990**, *90*, 320.